Volume 1 | Number 1 | Jan 2013 | Pages 1–100

Journal of
Materials Chemistry A

Materials for energy and sustainability
www.rsc.org/materialsA

Li⁺

ROYAL SOCIETY
OF CHEMISTRY

ROYAL SOCIETY
OF CHEMISTRY

www.rsc.org/materialsA

The table of contents entry

One type of nonlinear materials, $Na_3VO_2B_6O_{11}$ (NVB), demonstrates 90 times higher photocatalytic efficiency than that of the commercial P25 in dechlorination of 2, 4-DCP under UV-vis light irradiation.
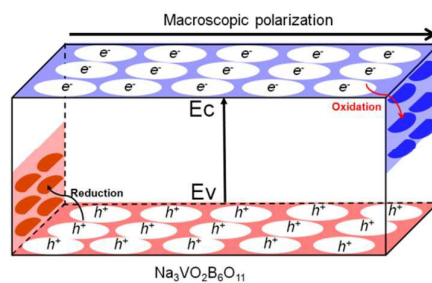
ARTICLE TYPE

Efficient Photocatalytic Dechlorination of Chlorophenols over a Nonlinear Optical Material Na₃VO₂B₆O₁₁ under UV-visible Light Irradiation

Xiaoyun Fan,[a]*** Kangrong Lai,**[a, b] **Lichang Wang,**[c] **Hengshan Qiu,**[a] **Jiao Yin,**[a] **Pengjun Zhao,**[a] **Shilie Pan,**[a]
5 **Jinbao Xu,**[a] **and Chuanyi Wang,**[a]***

One type of nonlinear optical crystal Na₃VO₂B₆O₁₁ (NVB) with noncentrosymmetry was synthesized and shows extraordinary UV-visible light driven photocatalytic activity in dechlorination of 2,4-DCP under
10 UV-vis ($\lambda > 320$ nm) light irradiation. The obtained dechlorination efficiency is 90 times higher than that of the commercial P25 TiO₂ catalyst under the same conditions. The noncentrosymmetric structure of NVB gives rise to an intrinsic large polarization effect as evidenced by Kelvin probe force microscopy, and the polarization promotes separation of photogenerated electron-hole pairs, leading to efficient cleavage of chlorophenols into phenol series fragments and dissociative Cl⁻ anions. A possible reaction
15 pathway for 2, 4-DCP dechlorination by NVB upon UV-vis light irradiation is proposed. Hydrodechlorination was found to be the major reaction pathway for 2,4-DCP dechlorination which could react with hydroxyl radicals to produce 1,4-benzoquinone and ocatechol. This work further advances the understanding of nonlinear optical materials, which opens up a new route to the design and synthesis of highly efficient photocatalysts by using nonlinear optical materials.

20 1. Introduction

Semiconductor materials, as a class of promising photocatalysts for organic pollutants treatment, have attracted increasing research interests in the past decades.[1] In principle, the overall efficiency of a photocatalytic reaction is determined by all three
25 steps: photo-excitation, charge separation and surface reactions; while in most cases, the overall efficiency is critically limited by the charge separation since about 90% of photogenerated charge carriers recombine together within very short time (~*ps*) after initial photo-excitation[2]. To improve photocatalytic activity of a
30 photocatalyst, many approaches have been adopted, including plasmonic photocatalysts[3] by loading metals (Ag,[4] Au,[5] Cu[6]) in semiconductor catalyst and multiple functional heterogeneous photocatalysts such as a *z*-scheme to mimic the natural photosynthesis,[7] which can provide trapping sites for the
35 photogenerated charges and promote the charge separation, thus enhancing the quantum efficiency. In addition, some novel catalysts have also been explored, such as, carbon nitrides (*g*-C₃N₄),[8] Ag₃PO₄,[9] graphene-based,[10] organic molecules,[11] and so on. Despite the significant interest and considerable efforts been
40 paid to date, the current research on photocatalysts is still far from satisfactory in terms of efficiency, stabilities and controlling carrier generation, separation and transportation.

Polar materials are featured by lacking of inversion center in crystal structure. Macroscopic polarization is generated when
45 dipolar units are integrated (not compensated) in some direction.[12] Materials with macroscopic polarization exhibit a variety of special properties, such as piezo-, pyroelectricity and second-order nonlinear optical activity.[13] A spontaneous polarization with directions pointing from the bulk to the surface
50 usually produces a positive charge on the surface (C⁺ domain), and the polarization pointing away from the surface to the bulk will generate a negative charge (C⁻ domain).[14] The spontaneous polarization can be screened by free electrons and holes, and/or by ions or molecules adsorbed on the surface from forming a
55 Stern layer.[15] This accumulation of free electrons on the C⁺ surface and holes on the C⁻ surface leads to downward and upward band bending, respectively.[16] The internal dipolar field creates charged surfaces that cause photogenerated charge carriers to move in opposite direction which separates electron-
60 hole pairs, leading to oxidation and reduction products formation at different locations.[17] Nonlinear optical crystals are known as non-concentric materials, however, their efficient charge separation and enhanced light absorption as a photocatalyst have rarely been reported.

65 B-O units, such as BO₃, BO₄, B₃O₆ and so on[18] have long been investigated as nonlinear optical (NLO) materials due to their rich structural chemistry.[19] On the other hand, Vanadium appears to be one of the best alternatives to improve visible light-driven photoactivity since it plays important role in extending optical
70 absorption region and the high separation efficiency of electron-hole pairs.[20] Herein, we demonstrate that a simple vandate-boron semiconductor, Na₃VO₂B₆O₁₁ (NVB), a kind of NLO materials, can function as an effective photocatalyst for dechlorination

under UV-visible light irradiation. Chlorophenols are typical hazardous organic pollutants utilized for timber and textile protection worldwide. They are listed as priority contaminants by China and the European Union.[21] In this work, 2, 4-dichlorophenol (2, 4-DCP) was selected as a model pollutant to test the photoactivity of NVB. The dechlorination efficiency is about 90 times higher than that of the commercial P25 TiO_2 catalyst. To the best of our knowledge, this is the first time to report the novel NVB single crystal material as a photocatalyst for dechlorination reactions.

2. Results and discussion

2.1. Structure and Optical Absorption

$Na_3VO_2B_6O_{11}$[22] (NVB) crystallizes in the space group $P2_12_12_1$ with cell dimensions $a = 7.7359(9)$ Å, $b = 10.1884(12)$ Å, and $c = 12.5697(15)$ Å, which is made of repeated B_6O_{11}, VO_4 units and Na ions as shown in Fig. 1.
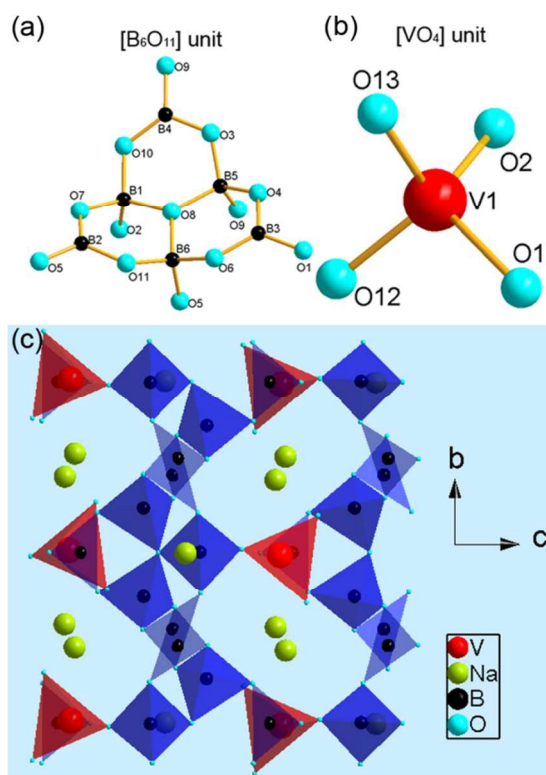

Fig. 1 Crystal structures of (a) B_6O_{11} units and (b) VO_4 units. (c) Drawing of the structure of NVB viewed down the a axis.

The basic building units of the NVB are trigonal planar BO_3 and tetrahedral BO_4, which form an isolated B_6O_{11} unit. The B_6O_{11} unit is connected with VO_4 tetrahedron to form infinite sheets, whereas Na^+ cations are distributed in the extended framework. The crystal structure of NVB is confirmed by XRD analysis (Fig. 2a). The UV-vis diffuse reflectance spectrum (Fig. 2b) indicates that the NVB particles can absorb photons in wavelength up to 419 nm, and the bandgap of NVB estimated from the intercept of the tangent to the inset plot of Fig. 2b is 2.95 eV.
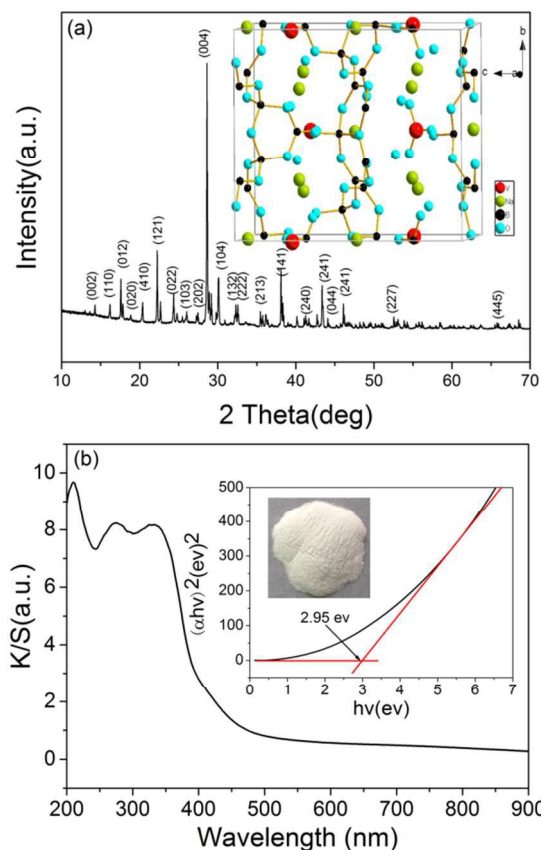

Fig. 2 (a) XRD patterns of the NVB powders. Inset: Schematic drawing of the crystal unit. (b) Ultraviolet-visible diffuse reflectance spectrum of the NVB sample. Inset: Plots of $(\alpha \times h\nu)2$ versus energy ($h\nu$) for the samples and the photograph of the photocatalyst.

2.2. Photocatalytic Performance of NVB nanoparticals

Experimental runs involving in the absence of the catalyst, with P25 and NVB under different wavelength of UV-visible irradiation were performed separately to evaluate each factor influencing the enhancement of photocatalytic degradation by NVB in Fig 3. One can observe in Fig. 3a that no obvious degradation took place in the absence of catalyst under UV-visible light. This is understandable considering that 2, 4-DCP degradation by oxygen flow is negligible. To explore the photocatalytic activity of the NVB samples for real applications, the photo-dechlorination of 2, 4-DCP was tested under natural sunshine. As shown in Fig. 3a, almost 43.85% of 2, 4-DCP can be dechlorinated by sunlight (Intensity = 0.05-0.08 w/cm² at noon) within 60 min, and complete dechlorination can be achieved in 3 min under UV-visible light irradiation (Intensity = 0.15 w/cm²) (Fig. 3a). During the dechlorination, a yellow color accumulated in the medium. This color is due to 5-chloro-2-hydroxymuconic semialdehyde (CHMS), the via-meta cleavage product of 4-chlorocatechol as also claimed by Farrell[23] and Sahinkaya[24]. An interesting observation is that CHMS concentration increases steadily with time course of degrading 2,4-DCP, as is also confirmed by LC-MS data and released chloride ion concentration. About 82.7% of the total chloride content is converted into Cl^- anions after 30 min of irradiation (Fig. 3b). The particle size of the crystals is in the range of 80-150 nm as

measured by scanning electron microscope (SEM) (Fig. S1). Furthermore, the Brunauer-Emmett-Teller adsorption analysis shows that the specific surface area of the NVB is 1.18 m^2g^{-1} (in the powder state). Such a small area value clearly indicates a high
5 photo-reactivity of the present NVB samples in nature. In dark within 20 min, the adsorption reached equilibrium, and about 15% of 2, 4-DCP was adsorbed onto NVB. Under the same conditions, about 6% of 2, 4-DCP was adsorbed onto P25 TiO_2. Considering that P25 TiO_2 has much bigger surface area (58 m^2g^{-1}), the higher
10 adsorptive capacity of NVB would be contributed by its surface charge properties other than the surface area.
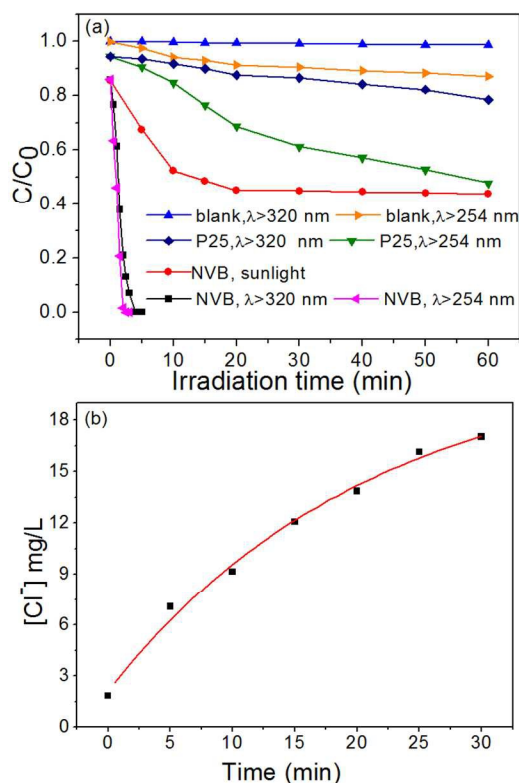

Fig. 3 (a) Photocatalytic dechlorination of 2, 4-DCP (50mg L-1, 100 mL) in aqueous dispersions (containing the NVB catalyst, 50 mg). (b)
15 Formation of Cl- as a function of irradiation time during the photo-dechlorination process under UV-vis light, source light wavelength λ > 320 nm.

The pH value is a complex parameter, since it is related to the state of the material surface as well as their redox potentials,
20 which affects the adsorption and reaction of DCP on the material. The effect of pH value on the photoreaction was investigated over NVB. The pH of point of zero charge (pH_{pzc}) value was measured as 4.94 for NVB. When the pH is near the pH_{pzc} of the semiconductor, most of the surface hydroxyl groups are in a
25 neutral state; nearly no surface charge exists.[25] Considering that the pKa of 2, 4-DCP is 7.85, it is in its undissociated form at the tested neutral pH values, and the surface of NVB is more favorable to the adsorption of 2, 4- DCP. As Shown in Fig. S2, the sample has higher degradation activity in acidic pH than in
30 alkaline pH solution. At pH 3 (adjusted with HCl), the NVB surface is positively charged which is more beneficial for adsorption of unionized 2, 4-DCP molecules (Fig. S2a). A similar enhancement of adsorption in acidic environment compared to

neutral media was also observed in case of phenol compounds.[25]
35 At pH 11 (adjusted with NaOH), which is above the pH_{pzc} of NVB, the photocatalyst surface is negatively charged. Under such conditions water molecules can block the photocatalyst surface thus giving rise to low adsorption ability and dechlorination activity of 2,4-DCP (Fig. S2b). The NVB sample retains
40 photocatalytic activity after four successive cycles of complete degradation 2, 4-DCP under UV-visible irradiation (Fig. S3). No peak change in the XRD patterns of NVB with the JCPDS Card (No. 52-0421) observed before and after the photodechlorination reaction (Fig. S4), indicating the stability of the NVB catalyst in
45 the present photocatalytic reaction process.

2.3. Calculations and Electron Transfer Mechanism

A bond valence approach has been adopted to evaluate the local dipole moments in NVB[26].

The calculations for trigonal $[BO_3]$ and tetrahedral $[BO_4]$ give
50 values of 0.277-1.482 D and 0.337-1.428 D [27], respectively. It is noteworthy that $[VO_4]$ polyhedra have a large negative charge which maintains a large dipole moment 5.548 D. A complete calculation of dipole moments for the constituted polyhedra is listed in Table S1. These B-O units possess large electron cloud
55 overlapping, and prefer to attract holes and repel electrons. Therefore, NVB can be easily polarized, thus facilitating separation of the photogenerated electron-hole pairs. This in turn enhances the photocatalytic activity.
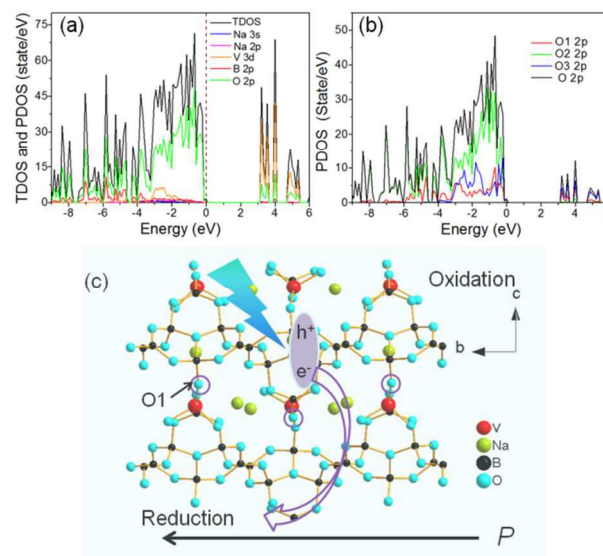

Fig. 4 The total and projected DOS plots calculated for (a) NVB and (b)
60 the different O atoms in NVB; (c) a schematic illustration showing the internal polarized field enhances the charge separation and the photocatalytic mechanism of NVB, one of the O atoms is labeled by a purple circle.

65 To get a deeper understanding of the high photoactivity of NVB, we have performed density functional theory (DFT) calculations. Fig. 4 presents the electronic band structure of NVB in terms of density of states (DOS). The VB has strong O 2p contributions, while the CB has V3d contributions (Fig. 4a).
70 There are three types of oxygen atoms in NVB: the O1 atoms belong to the bridge between VO_4 unit and B_6O_{11} unit, while the O2 atoms form the VO_4 unit, and the O3 atoms belong to B_6O_{11} unit. The VB top has O 2p contributions, and O1 and O3 atoms

have similar contribution values (Fig. 4b). Therefore, photoexcitation from the VB top to the CB generates holes at the O 2p states in all O atoms, especially in O2. On the other hand, the CB bottom has V 3d primary contributions and O3 2p
5 secondary contributions from B_6O_{11} unit, thus the photogenerated electrons can be gathered in B_6O_{11} unit and cease at the p-states of the V $^{5+}$ sites (Fig. 4c). As described in Fig. 4c, with a polar electric field in the crystal structure of NVB, photogenerated charges at B_6O_{11} unit can migrate through the O1 atoms (circled
10 in purple) to adjacent VO_4 unit, and vice versa. When electrons and holes are separated at B_6O_{11} units, electrons can move to adjacent VO_4 unit by means of the bridging O1 whose contribution to the CB is present, while holes can be trapped in O3 because of their vertical orientation with the direction of the
15 internal polar field or maintained at O3. In a similar manner, the photogenerated holes at B_6O_{11} units can move through the bridging O1 to the VO_4 units and eventually be immobilized on the O2 atoms of VO_4 units, while the photogenerated electrons might end up in V 3d at the CB bottom. In general, electrons and
20 holes are gathered at B_6O_{11} units and VO_4 units, respectively, separated along the *b* axis. Furthermore, for the crystallographic non-centrosymmetry structure of NVB, with the ordered arrangement of the units in crystal structures, the direction of the dipole moment is along the [010] direction, an internal polar field
25 is verified to be existed and its orientation is shown in Fig. 5a. From the crystal structure of NVB, the direction of the polar field is in accordance with that of charge transfer in VO_4, the internal polar field promotes their separation along the field direction in the *bc* plane (Fig. 5a), which is expected to function as a driving
30 force for the photoexcitetd holes and electrons to move to their respective reduction and oxidation sites. Under the action of the internal polar field, the photoinduced electron and hole would thereby transfer along opposite directions, and facilitate the charge separation, thus resulting in high photocatalytic activity.
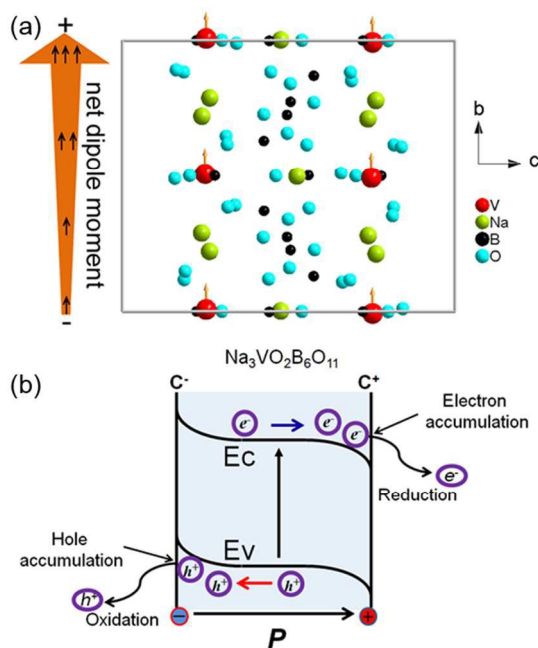

35 **Fig. 5** (a) Ball-and-stick diagram of NVB structure (orange arrows indicate the direction of the dipole moments for NVB units). (b) Schematic illustration of a polar structured NVB photocatalyst.

To evaluate the built-in electric field induced photocatalytic
40 activity of NVB, the dechlorination of 2, 4-DCP was further carried out in aqueous dispersions under different wavelengths of light irradiation after the adsorption of 2, 4-DCP onto the NVB (Fig. 3). When irradiated at wavelengths λ >254 nm, the rate of 2, 4-DCP dechlorination on NVB is nearly 90 times faster than that
45 on P25 TiO_2. Under irradiation of photons with wavelengths λ > 320 nm from a Xenon lamp, in the first 10 minutes no significant dechlorination occurs on P25 TiO_2, which hardly absorbs photons in these wavelengths range; while NVB exhibits almost the same photocatalytic activity as that at λ>254 nm. These results indicate
50 that the enhanced dechlorination of 2, 4-DCP is due to the internal dipolar field of NVB nano-particles which facilitate the excited electron-hole separation. Upon irradiation with photoenergy above the bandgap, electron-hole pairs are formed, which causes a restructuring of the conduction and valance band
55 bending. The resultant electrons and holes then migrate to their most energetically favored corresponding positions in the system, where they can accumulate, decay to the ground state, or take part in a chemical reaction (Fig. 5b). Therefore, internal electric field is critical to the enhanced activity of NVB.

60 **2.4. Internal Electric Field Effect**

The internal electric field effect was also studied with a nanoscale resolution by atomic force microscopy (AFM) in conjunction with Kelvin probe force microscopy (KPFM). In particular, KPFM allows quantitative mapping of the electronic properties of
65 nanostructures, i.e., determination of the surface potential of nano-objects.[28] Fig. 6a and 6c shows an AFM topography image of NVB nanoparticles, and Fig. 6b and 6d show surface potential images of NVB particles in the dark and under irradiation. The surface potential image has been separated into darker and
70 brighter regions. The contrast is due to the differences in surface potential for the domains of respective donor rich and acceptor rich of the material.

In order to quantitatively determine surface potential differences, the different potential value for Fig. 6b and 6d of the
75 NVB was analyze in Fig. 6e. Upon irradiation with a Xenon lamp light, the surface potential of the NVB becomes more positive and the average value increases by about 14.09 mV. This overall increase in surface potential is due to the filling of electrons in the conduction band during the light excitation process. And the
80 cross section profiles with the same area circled in a white square frame in Figs. 6b and 6d is shown in Fig. 6f, from which the surface potential difference between different faces due to the charge separation is deduced to be ∼30 mV. The difference is attributed to the light response for different domains of the
85 material, and after light irradiation the charge separation is driven by the internal electric fields. This result provides direct evidence that the presence of the internal field provides a driving force for the separation of photogenerated electrons and holes.[29] These properties strongly depend on that the crystal form for NVB is a
90 non-centric crystal. Thus, the KPFM results demonstrate that the excellent electron-hole separation of NVB can be significantly improved through the enhancement in charge injection and extraction.
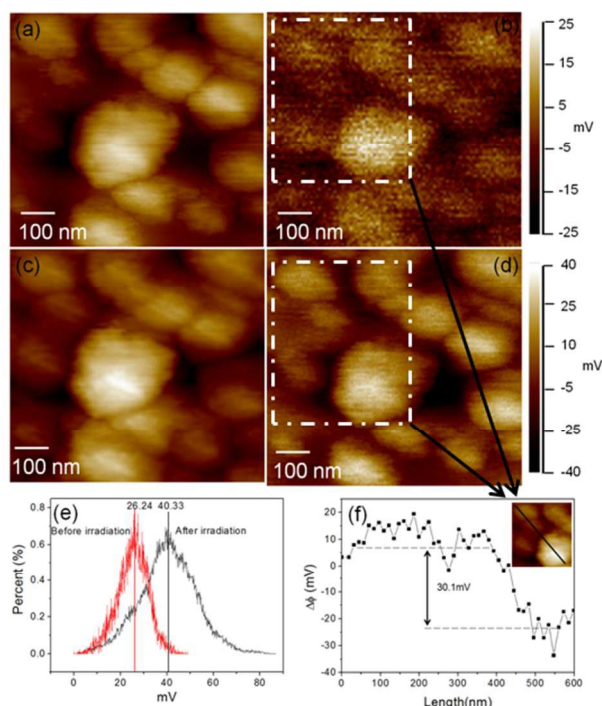
Fig. 6 AFM images of NVB before (a) and after (c) irradiation and corresponding surface potential images of NVB before (b) and after (d) irradiation. (e) Potential value curve for panel (b) and panel (d). f) Surface potential profile along the black line inset of (f), by subtracting the potential value of panel (d) from panel (c) in the white circled area.

2.5. Enhancement of PC and PEC activity

In order to further confirm that the photon-to-electron conversion efficiency of the NVB particles is affected by the non-centric structure, the photoelectron chemical (PEC) measurements of the NVB photoanodes have been conducted.[30] The transient photocurrent responses of P25 TiO$_2$ and NVB electrodes were recorded via several on-off cycles of irradiation.

It can be seen from Fig. 7a that a prompt generation of photocurrents occurs with good reproducibility when sample NVB is irradiated by UV-visible light. While the light is off, the photocurrent for sample NVB decreases instantaneously. This indicates that under light irradiation, most of the photoexcited electrons at the NVB surface due to internal electric field are transported towards the desired reactions. When the bias potential is 0 V, the anodic photo-current of NVB is about 3.2 times of that of P25 TiO$_2$ in the simulated UV-vis light irradiation. As the bias potential increases, the photocurrents are enhanced by 1.3, 1.7 and 1.9 times at 0.033, 0.067 and 0.134 V compared to 0 V, respectively, for NVB electrode as shown in Fig. 7b. This suggests any photocurrent enhancement observed for NVB is more significant at lower potentials which contributes to its catalytic ability towards organic pollutants degradation.
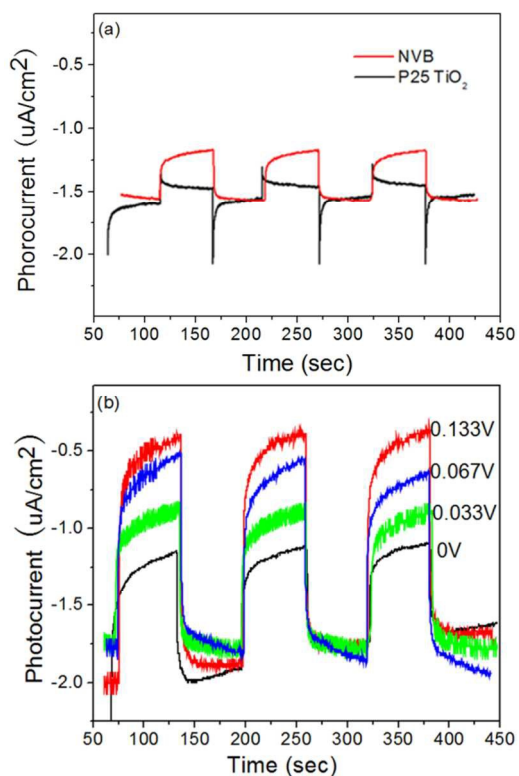

Fig. 7 (a) P25 TiO$_2$ and NVB light on- off experiment using a 300W Xenon lamp (150 mW/cm^2) by the removal of 2, 4-DCP (with an initial concentration of 50 mg/L) in 0.1 M Na2SO4 solution. (b) Electrode at 0 V, 0.033 V 0.067 V and 0.134 V of NVB vs. Ag/AgCl .

Photoelectrochemical impedance spectroscopy (PEIS) analysis was employed to investigate the charge transfer at the semiconductor interface.[31] A Nyquist plot for NVB and P25 TiO$_2$ measured at 0.067 V vs. Ag/AgCl under different wavelength irradiations are shown in Fig. 8. With wavelength λ>320 nm light irradiation, the impedance arcs of the two electrodes are large, indicating that the electrons going through the electrode and electrolyte interface are few. However, arcs obtained from NVB have much smaller radius than from P25 TiO$_2$, which indicates that NVB has an more effective separation of photogenerated electron-hole pairs resulting in faster interfacial charge transfer.[32] Under UV-vis light irradiation (λ>254 nm), the arc radius on the EIS Nyquist plot of NVB is also smaller than that of P25 TiO$_2$. It can be deduced that UV-vis light irradiation facilitates photogenerated holes transfer from the valence band of NVB to the solution, reducing the recombination of photogenerated electron-hole pairs and improving the photocurrent density. The efficiency of NVB is higher compared to that of P25 TiO$_2$ electrodes. This could be attributed to the improved electrode-electrolyte interfacial area due to the presence of polarity in NVB arisen from its noncentric symmetry structure.
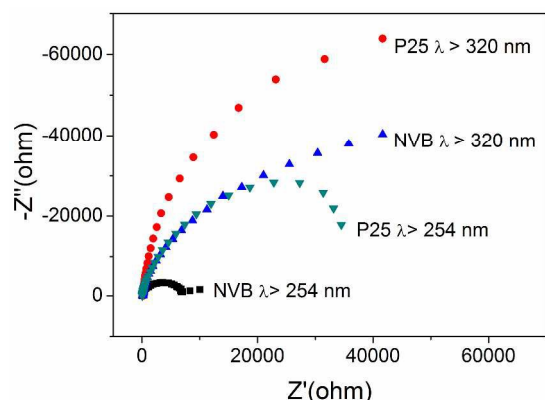
Fig. 8 EIS Nyquist plots of the P25 TiO₂ and NVB electrodes under UV and UV-visible-light irradiation. The bias potential is 0.067 V.

2.6. Possible Reaction Mechanism for DCP Photodechlorination

As reported by Cheng *et al*[33]., the reaction pathway for 2, 4-DCP dechlorination could involve adsorption, dechlorination and cleavage of the benzene ring and several intermediates including 2-chlorophenol, 4-chlorpheol, phenol, and chlor-ocatechol. To elucidate the reaction pathways of DCP by NVB, LC-MS was used to identify the intermediates and end products. Degradation intermediates including 2-chlorohydroquione, 4-chlorophenol and catechol were identified, while 1,4-benzoquine and catechol were detected as the end products during the course of 2,4-DCP photodechlorination (see Supplementary Information Fig. S5 and Table S2 for details). Therefore, a possible reaction pathway for 2, 4-DCP dechlorination by NVB upon UV-vis light irradiation is proposed (Fig. S6). As shown in Fig. S6, 2,4-DCP can react with photo-generated hydroxyl radicals to form 2-chlorohydroquinone and then to 1, 4-benzoquinone. In addition, 2,4-DCP can undergo reductive dechlorination to generate 4-chlorophenol first and then reacts with hydroxyl radicals, leading to the formation of catechol and phenol. Although 2,4-DCP cannot be completely mineralized by NVB, the degradation intermediates as well as end products are less toxic than that of 2,4-DCP and can be readily biodegraded into harmless compounds by microorganisms under both aerobic and anaerobic conditions.[34]

The enhanced photo-dechlorination of chlorinated compounds by NVB is illustrated in Scheme 1. The NVB photocatalysts can be photo-excited by UV-visible ($\lambda > 320$ nm) light irradiation to generate electron-hole pairs, while the strong built-in electric field in NVB structure inhibits the recombination of holes with electrons, leading to the enhancement of the oxidizing capability of NVB. This process would significantly accelerate the simultaneous photodechlorination rates of chlorinated compounds.
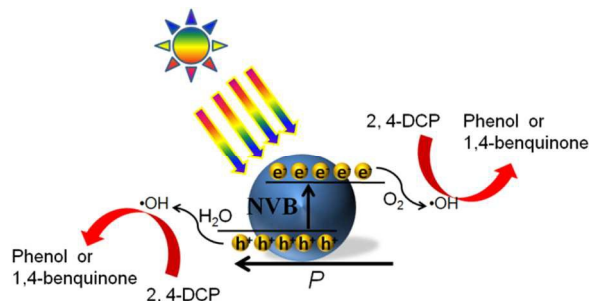
Scheme 1. The enhanced photodechlorination efficiency of 2,4-DCP by NVB materials upon irradiation of UV-visible light ($\lambda > 320$ nm) under anoxic conditions.

To further explore the photocatalytic reaction pathway of NVB, the formation of active hydroxyl radicals (•OH) upon irradiation was monitored, which are generally considered as the most important oxidative intermediate in photocatalytic reactions.[35] Tereph-thalic acid (TA) was used as a fluorescence probe which can react with •OH in basic solution to generate 2-hydroxy terephthalic acid (TAOH), emiting unique fluorescence signal at around 426 nm.[36]

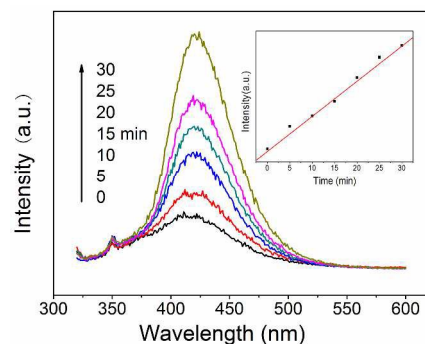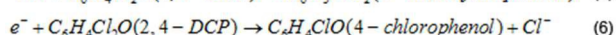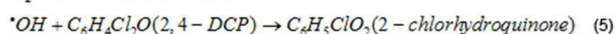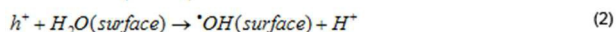**Fig. 9** Hydroxyl radical •OH trapping photoluminescence (PL) spectra of NVB in TA solution under UV-visible-light irradiation. Insert: Plot of the induced PL intensity (at 426 nm) vs irradiation time.

As shown in Fig. 9, intense fluorescence signals associated with 2-hydroxy terephthalic acid (TAOH) are generated upon irradiation of NVB suspended in terephthalic acid (TA) solution within 220-770 nm with different irradiation durations. The quasi-linear relationship between fluorescence intensity and irradiation time (inset of Fig. 9) confirms the stability of NVB. Taking all together, the dechlorination processes of 2,4-DCP at NVB are proposed in Equations 1-6 as following:

$$NVB \rightarrow NVB(e^- + h^+) \tag{1}$$

$$h^+ + H_2O(surface) \rightarrow {}^\bullet OH(surface) + H^+ \tag{2}$$

$$e^- + O_2(surface) \rightarrow O_2^{\bullet-} \tag{3}$$

$$O_2^{\bullet-} + H^+ \rightarrow HOO^\bullet \rightarrow {}^\bullet OH \tag{4}$$

$${}^\bullet OH + C_6H_4Cl_2O(2-DCP) \rightarrow C_6H_5ClO_2(2-chlorhydroquinone) \tag{5}$$

$$e^- + C_6H_4Cl_2O(2-DCP) \rightarrow C_6H_4ClO(4-chlorophenol) + Cl^- \tag{6}$$

3. Experimental

3.1. Synthesis of the NVB nanoparticles

Nanoparticles of NVB were synthesized by a high temperature solid-state reaction method. Stoichiometric amounts of Na₂CO₃ (Tianjin Benchmark Chemical Reagent Co., Ltd., 99.8%), V₂O₅

(Shanghai Shanpu Chemical Co., Ltd., 99.5%), and H_3BO_3 (Tianjin Baishi Chemical Industry Co., Ltd., 99.5%) were ground together and then placed in an alumina crucible and heated at 600 °C for 10 h in air in a tube furnace followed by natural cooling.

3.2. Photoactivity evaluation

Photocatalytic activity tests for all samples were carried out at room temperature. During the experiment, 50 mg of NVB sample was dispersed in 100 mL of 2, 4-DCP solution (50 mg/L) in a reactor and stored for 20 min with stirring in the dark to attain adsorption equilibrium. The reactor was then illuminated by a 300 W Xenon lamp with a wavelength range of 320-780 nm (The intensity at the test samples = 0.15 w/cm^2). Samples were withdrawn periodically from the reactor. The percentage of residual 2, 4- DCP solution at a selected time of irradiation is given by C/C_0, where C_0 is the concentration of the 2, 4- DCP solution at initial stage, i.e., right before irradiation, and C is the concentration at selected irradiation times of time = 0, 1, 2, 3, 4 and 5 min. For comparison, parallel experiments were conducted with P-25. Adopting the same procedures, a 500 W Mercury lamp with wavelength λ> 254 nm was also employed for comparison.

3.3. Characterization

Phase identification was performed on a Bruker D8 ADVANCE X-ray diffractometer equipped with a diffracted-beam monochromator set for Cu Kα radiation (λ = 1.5418 Å). The morphologies of the samples were observed on a scanning electron microscope (SEM) using a ZEISS SUPRA55VP apparatus. UV-visible diffuse reflectance spectra were recorded on a Shimadzu UV-3600 UV-vis spectrophotometer using $BaSO_4$ as a reference. BET measurements were conducted by a Quantachrome Autosorb-2 apparatus at 77.35 K. The concentration of chlorophenol was measured by UV-vis spectroscopy (Shimadzu Uv-1800) and using high-performance liquid chromatography (Ultimate 3000; Dionex) with a Supelco PAH column (4.6× 250 mm). A mixture of acetonitrile, water, and acetic acid [60/39.75/ 0.25 (v/v/v)] was used as an effluent, and the flow rate was 1.0 mL/min. The intermediate products during 2,4-DCP degradation were qualitatively analyzed by a liquid chromatography-mass spectrometry (LC-MS, Agilent 1290). The size of the sample loop was 20 mL. The wavelength of the detector was set at 282 nm. To determine the concentration of chloride ions (Cl$^-$), an ion chromatography (ICS2000, Dionex, Germany) equipped with an analytical column (4 mm × 250 mm) and a guard column (4 mm × 50 mm) was used throughout the experiment. The eluent was 3.5 mM Na_2CO_3 and 1.0 mM $NaHCO_3$ with a flow rate of 1.0 mL/min.

Atomic force microscope (AFM) combined with Kelvin probe force microscopy (KPFM) measurements were performed at room temperature with an atomic force microscope (AFM) (Bruker Multimode 8). Every scan took approximaterly 20 min from top to bottom, which is the time scale to refer to in this experiment. Images were obtained in tapping mode with a scan rate of 1 Hz by a conductive Pt-Ir tips (SCM-PIT) with the resonance frequency of 60-100 kHz and an AC mode for a scan size of 1 μm × 1 μm. In the experiment, NVB nanoparticles were first dispersed in water and then sprayed on a Pt substrate to form a film. Before measurements, the sample was baked in a dry oven at 400 °C for 2 h. For the light irradiation experiment, a Xenon

lamp with a wavelength (λ) of >320 nm and a convex lens with a focusing spot size (d) of 1.5 cm was used to introduce focused UV light onto the measurement region between the tip of the atomic force microscope and sample.

The photocurrents of UV-vis light on and off studies were performed on a CHI660E electrochemical system (Shanghai, China) using a standard three-electrode cell with a working electrode (20 mm×20 mm), a platinum plate as counter electrode, and a standard calomel electrode (SCE) as reference electrode. PEC measurements were performed using a three-electrode configuration by the removal of 2, 4-DCP (with an initial concentration of 50 mg/L) in an aqueous solution containing 0.1 M Na_2SO_4. The transient photocurrent responses of P25 TiO_2 and NVB electrodes were recorded via several on-off cycles of irradiation. Electrochemical impedance spectroscopy (EIS) measurements carried out by an electrochemical workstation (Zahner Im6ex) were conducted for the working electrode in a frequency range of 100 kHz to 0.01 Hz with ac signal amplitude of 5 mV at open circuit potential in different aqueous electrolytes.

Fluorescence spectra of 2-hydroxyterephthalic acid were measured on a Hitachi fluorescence spectrophotometer F-7000. The •OH radical trapping experiments were carried out using the following procedure: terephthalic acid (TA) (16.6 mg) was first dissolved in 200 mL of dilute NaOH solution (2×10^{-3} M), followed by addition of 100 mg of photocatalysts, and stirred for 30 min in dark. The suspension was irradiated by a 300 W xenon lamp at wavelengths in the range of 320-780 nm for 30 min. The fluorescence emission spectrum of the solution was measured every 5 min during irradiation. At a defined time interval, the concentration of solution in the system was analyzed by PL (excited at 312 nm).

3.4. Computational details

The first-principles calculations were performed in the framework of functional theory with the projector augmented wave (PAW) [37] pseudopotential method using Vienna ab initio Simulation Package (VASP) [38]. The generalized gradient approximation (GGA) [39] in the scheme of the Perdew-Burke-Ernzerhof (PBE) [40] was used for the exchange-correlation functional. The electronic wave functions were expanded into a basis set of plane waves with a kinetic energy cutoff of 400 eV, and a Monkhorst-Pack k-point mesh of 3×2×2 was used for geometry optimization and electronic property calculations, which was found to be sufficient to reach convergence for bulk super cell calculations. The PAW potentials with the valence states 2s and 2p for B and O, 3s and 2p for Na, 3p, 4s, and 3d for V, were employed. Both the atomic positions and cell parameters were optimized until the residual forces experienced by each ion converged to be smaller than 0.02 eV/Å, and the convergence threshold for self-consistence-field iteration was set at 10^{-5} eV. The experimental atomic positions were employed as the starting points of relaxation, and subsequent calculations were conducted using the relaxed atomic positions.

4. Conclusion

In summary, one type of nonlinear optical crystal $Na_3VO_2B_6O_{11}$ (NVB) with noncentrosymmetry was synthesized by a high temperature solid state method. As-synthesized NVB shows

extraordinary UV-visible light driven photocatalytic activity, giving high efficiency in dechlorination of 2,4-DCP under UV-vis (λ > 320 nm) light irradiation. The obtained dechlorination efficiency is 90 times higher than that of the commercial P25 TiO$_2$ catalyst under the same conditions. The strong built-in electric field in NVB structure can effectively separate and transfer photo-induced charge carriers. A possible reaction pathway for 2,4-DCP dechlorination by NVB upon UV-vis light irradiation is proposed. Hydrodechlorination was found to be the major reaction pathway for 2,4-DCP dechlorination, and 2,4-DCP could react with hydroxyl radicals to produce 1,4-benzoquinone and ocatechol. Furthermore, NVB exhibits the capability for generating critical active species of •OH radicals in photocatalysis, which could be useful for the enhanced degradation of co-contaminants in the aquatic environment. This work further advances the understanding of nonlinear optical materials, which opens up a new route to the design and synthesis of highly efficient photocatalysts by using nonlinear optical materials.

Acknowledgements

Notes and references

^{a} Laboratory of Environmental Sciences and Technology, Xinjiang Technical Institute of Physics & Chemistry; Key Laboratory of Functional Materials and Devices for Special Environments, Chinese Academy of Sciences, Urumqi 830011, China. Fax: Fax: +86 0991 383 8957; Tel: +86 0991 383 5879; E-mail: xyfan@ms.xjb.ac.cn; cywang@ms.xjb.ac.cn
^{b} Department of Physics, Changji University, Changji 831100, China
^{c} Department of Chemistry and Biochemistry, Southern Illinois University, 1245 Lincoln Dr Carbondale, IL 62901. Fax: 61 8453 6408; Tel: 61 8453 6476; E-mail: lwang@chem.siu.edu

† Electronic Supplementary Information (ESI) available: [*Bond valences and dipole moments calculations, SEM measurements, dechlorinations at NVB under different pH values, repeated degradation cycles at NVB and NVB XRD pattern differences with photoreactions as* Supplementary Information]. See DOI: 10.1039/b000000x/

‡ Footnotes should appear here. These might include comments relevant to but not central to the matter under discussion, limited experimental and spectral data, and crystallographic data.

1   M. R. Hoffmann, S. T. Martin, W. Choi and D. W. Bahnemann, *Chem. Rev.*, 1995, **95**, 69.
2   (a) J. He, G. Benkö, F. Korodi, T. Polívka, R. Lomoth, B. Åkermark, L. Sun, A. Hagfeldt and V. Sundström, *J. Am. Chem. Soc.* 2002, **124**, 4922; (b) A. Fujishima, X. Zhang and D. A. Tryk, *Surf. Sci. Rep.*, 2008, **63**, 515; (c) N. Aiga, Q. Jia, K. Watanabe, A. Kudo, T. Sugimoto and Y. Matsumoto, *J. Phys. Chem. C*, 2013, **117**, 9881; (d) K.-i. Yamanaka, S. Sato, M. Iwaki, T. Kajino and T. Morikawa, *J. Phys. Chem. C*, 2011, **115**, 18348.
3   (a) Q. Xiang, J. Yu and M. Jaroniec, *Chem. Soc. Rev.*, 2012, **41**, 782; (b) Q. Zhang, D. Q. Lima, I. Lee, F. Zaera, M. Chi and Y. Yin, *Angew. Chem. Int. Ed.*, 2011, **123**, 7226; (c) M. J. Kale, T. Avanesian and P. Christopher, *Acs Catal.*, 2013, **4**, 116; (d) R. Jiang, B. Li, C. Fang and J. Wang, *Adv. Mater.* 2014, **26**, 5274.
4   J. Li, S. K. Cushing, J. Bright, F. Meng, T. R. Senty, P. Zheng, A. D. Bristow and N. Wu, *Acs Catal.*, 2012, **3**, 47.
5   J. Li, S. K. Cushing, P. Zheng, F. Meng, D. Chu and N. Wu, *Nat. Commun.*, 2013, **4**,1444.
6   G. H. Chan, J. Zhao, E. M. Hicks, G. C. Schatz and R. P. Van Duyne, *Nano. Lett.*, 2007, **7**, 1947.
7   (a) Y. Sasaki, H. Kato and A. Kudo, *J. Am. Chem. Soc.*,2013, **135**, 5441; (b) K. Maeda, *Acs Catal.*, 2013, **3**, 1486.
8   (a)X. Wang, K. Maeda, A. Thomas, K. Takanabe, G. Xin, J. M. Carlsson, K. Domen and M. Antonietti, *Nat. Mater.*, 2009, **8**, 76; (b) S. C. Yan, Z. S. Li and Z. G. Zou, *Langmuir*, 2009, **25**, 10397; (c) G. Dong, K. Zhao and L. Zhang, *Chem. Commun.*, 2012, **48**, 6178; (d) X.-H. Li, X. Wang and M. Antonietti, *Chem. Sci.*, 2012, **3**, 2170.
9   (a) Z. Yi, J. Ye, N. Kikugawa, T. Kako, S. Ouyang, H. Stuart-Williams, H. Yang, J. Cao, W. Luo, Z. Li, Y. Liu and R. L. Withers, *Nat. Mater.*, 2010, **9**, 559; (b) Y. Qu, R. Cheng, Q. Su and X. Duan, *J. Am. Chem. Soc.*, 2011, **133**, 16730.
10   (a) N. Zhang, Y. Zhang and Y.-J. Xu, *Nanoscale*, 2012, **4**, 5792; (b) P. V. Kamat, *J. Phys. Chem. Lett.*, 2011, **2**, 242; (c) Q. Xiang and J. Yu, *J. Phys. Chem. Lett.*, 2013, **4**, 753.
11   D. M. Schultz and T. P. Yoon, *Science*, 2014, **343**.
12   R. Resta, *Rev. Mod. Phys.*, 1994, **66**, 899.
13   (a)T. Goldacker, V. Abetz, R. Stadler, I. Erukhimovich and L. Leibler, *Nature*, 1999, **398**, 137; (b) X. Ren, *Nat. Mater.*, 2004, **3**, 91; (c) R. Su, Y. Shen, L. Li, D. Zhang, G. Yang, C. Gao and Y. Yang, *Small*, 2015, **11**, 202.
14   S. Dunn, P. M. Jones and D. E. Gallardo, *J. Am. Chem. Soc.*, 2007, **129**, 8724.
15   Y. Cui, J. Briscoe and S. Dunn, *Chem. Mater.*, 2013, **25**, 4215.
16   L. Li, P. A. Salvador and G. S. Rohrer, *Nanoscale*, 2014, **6**, 24.
17   S. T. Kochuveedu, Y. H. Jang and D. H. Kim, *Chem. Soc. Rev.*, 2013, **42**, 8467.
18   C. Chen, N. Ye, J. Lin, J. Jiang, W. Zeng and B. Wu, *Adv. Mater.*, 1999, **11**, 1071.
19   H. Wu, S. Pan, K. R. Poeppelmeier, H. Li, D. Jia, Z. Chen, X. Fan, Y. Yang, J. M. Rondinelli and H. Luo, *J. Am. Chem. Soc.*, 2011, **133**, 7786.
20   (a) W. J. Jo, J.-W. Jang, K.-j. Kong, H. J. Kang, J. Y. Kim, H. Jun, K. P. S. Parmar and J. S. Lee, *Angew. Chem. Int. Ed.*, 2012, **124**, 3201; (b) J. Yu and A. Kudo, *Adv. Funct. Mater.*, 2006, **16**, 2163; (c) T. W. Kim and K.-S. Choi, *Science*, 2014, **343**, 990.
21   U. G. Ahlborg, T. M. Thunberg and H. C. Spencer, *Crit. Rev. Toxicol.*, 1980, **7**, 1.
22   P. E. Blöchl, *Phys .Rev. B*, 1994, **50**, 17953.
23   (a) G. Kresse and J. Hafner, *Phys .Rev. B*, 1993, **47**, 558; (b) G.Kresse and J. Furthmüller, *Phys .Rev. B*, 1996, **54**, 11169.
24   J. P. Perdew and Y. Wang, *Phys .Rev. B*, 1992, **45**, 13244.
25   J. P. Perdew, K. Burke and M. Ernzerhof, *Phys. Rev. Lett.*, 1996, **77**, 3865.
26   X. Fan, S. Pan, X. Hou, X. Tian, J. Han, J. Haag and K. R. Poeppelmeier, *Cryst. Growth Des.*, 2009, **10**, 252.
27   A. Farrell and B. Quilty, *Biodegradation*, 1999, **10**, 353.
28   E. Sahinkaya and F. B. Dilek, *J. Hazard. Mater.*, 2006, **137**, 282.
29   Saber Ahmed, M.G. Rasul, Wayde N. Martens, R. Brown and M. A. Hashib., *Desalination*, 2010, **261**, 16.
30   (a) I. D. Brown and D. Altermatt, *Acta Crystallogr. Sect. B*, 1985, **41**, 244; (b) N. E. Brese and M. O'Keeffe, *Acta Crystallogr. Sect. B*, 1991, **47**, 192.
31   Z. Lou, B. Huang, Z. Wang, X. Ma, R. Zhang, X. Zhang, X. Qin, Y. Dai and M.-H. Whangbo, *Chem. Mater.*, 2014, **26**, 3873.
32   (a) P. Samori, *Chem. Soc. Rev.*, 2005, **34**, 551; (b) V. Palermo, M. Palma and P. Samorì, *Adv. Mater.*, 2006, **18**, 145; (c) O. Kolosov, A. Gruverman, J. Hatano, K. Takahashi and H. Tokumoto, *Phys. Rev. Lett.*, 1995, **74**, 4309.
33   J. N. Hanson, B. J. Rodriguez, R. J. Nemanich and A. Gruverman, *Nanotechnology*, 2006, **17**, 4946.

34   S. K. Pilli, T. E. Furtak, L. D. Brown, T. G. Deutsch, J. A. Turner and A. M. Herring, *Energ. Environ. Sci.*, 2011, **4**, 5028.
35   Q. Kang, J. Cao, Y. Zhang, L. Liu, H. Xu and J. Ye, *J. Mater. Chem. A*, 2013, **1**, 5766.
36   (a) Y. Hou, F. Zuo, A. Dagg and P. Feng, *Angew. Chem. Int. Ed.,* 2013, **52**, 1248; (b) B. Klahr, S. Gimenez, F. Fabregat-Santiago, J. Bisquert and T. W. Hamann, *Energ. Environ. Sci.*, 2012, **5**, 7626.
37   G. K. Parshetti and R.-a. Doong, *Water. Res.*, 2011, **45**, 4198.
38   D.-S. Shen, X.-W. Liu and H.-J. Feng, *J. Hazard. Mater.,* 2005, **119**, 239.
39   T. Hirakawa and Y. Nosaka, *Langmuir*, 2002, **18**, 3247.
40   J. C. Yu, Yu, Ho, Jiang and Zhang, *Chem .Mater.,* 2002, **14**, 3808.